

ReN₂ monolayers as electrode materials for Na- and K-ion batteries

Shi-Hao Zhang^{†,‡} and Bang-Gui Liu^{*,†,‡}

[†]*Beijing National Laboratory for Condensed Matter Physics, Institute of Physics, Chinese Academy of Sciences, Beijing 100190, China*

[‡]*School of Physical Sciences, University of Chinese Academy of Sciences, Beijing 100190, China*

E-mail: bgliu@iphy.ac.cn

Abstract

Searching for good two-dimensional electrode materials with both high capacity and low diffusion barriers is necessary to the alkali metal-based batteries. Here, we propose ReN₂ monolayer as a new two-dimensional material, with a buckled tetragonal structure, for this purpose. Calculated phonon spectrum and elastic moduli prove its dynamical and mechanical stability, and our elastic theoretical analysis shows that it can exist without the support of substrate. Our investigation shows that it is metallic and still keep metallic feature after the adsorption of Na or K atoms, and its maximum capacity reaches 751 mA h g⁻¹ for Na-ion batteries and 250 mA h g⁻¹ for K-ion batteries. Its lattice parameter changes by only 3.2% or 3.8% after absorption of such Na or K atoms. Its diffusion barrier is only 0.027 eV for Na atom and 0.127 eV for K atom. The high capacity, small lattice change, metallic feature, and extremely low diffusion barriers make the ReN₂ monolayer become promising electrode materials for Na-ion rechargeable batteries with ultrafast charging/discharging processes.

Introduction

Recent years have witnessed a booming development in two-dimensional materials since the experimental discovery of graphene.¹⁻⁴ Besides graphene, such two-dimensional materials as phosphorene and transition-metal dichalcogenides (TMDC) exhibit many novel physical properties which do not exist in their bulk counterparts. The two-dimensional materials are promising for applications in many fields, such as field-effect transistors,^{5,6} phototransistors,^{7,8} p-n junctions,^{9,10} supercapacitors,^{11,12} and batteries.^{13,14}

Since the commercialization of the lithium-ion batteries by Sony in 1991, rechargeable lithium-ion batteries have attracted increasing interest.¹⁵⁻²³ However, the Li-ion batteries need to face the problems: less idealistic reversibility, large volume change, and low diffusivity.²⁴⁻²⁶ Thus it is necessary to develop new anode materials. Because of the more natural abundance of Na (23000 ppm) and K (17000 ppm) than Li (20 ppm) in the earth's crust,²⁷ Na-ion and K-ion batteries have attracted much attention. To date, a tremendous number of 2D materials, including graphene systems,²⁸⁻³⁰ transition-metal dichalcogenides,³¹⁻³³ transition-metal carbides,³⁴⁻³⁶ and metal nitrides,³⁷ have been studied because of their excellent electrochemical performance as battery anode materials. The capacity of most two-dimensional materials is between 200 and 600 mA h g⁻¹ and the diffusion barrier is in the range of 0.1-0.6 eV. It is still necessary to seek good materials for Na-ion and K-ion batteries with both high capacity and low diffusion barrier.

Here, through first-principles calculation we study the two-dimensional crystal structures of ReN₂ monolayers and their electronic and mechanical properties. We obtain the stable tetragonal structure of ReN₂ monolayer in terms of our calculated phonon spectra and in-plane stiffness constants. According to elastic theory, the tetragonal ReN₂ can be freestanding without the support of substrate. Our calculations with the PBE functional and HSE functional with/without the spin-orbit coupling show that the ReN₂ monolayer is metallic. After the absorption of Na and K atoms, the system still keep the metallic feature which is advantageous for the applications in Na-ion and K-ion batteries. The capacity of

the ReN_2 monolayer is 751 mA h g^{-1} or 250 mA h g^{-1} when serving as Na-ion and K-ion anode materials, and the corresponding ion diffusion barrier, 0.027 eV for Na or 0.127 eV for K, is very small. The high capacity and the extremely low diffusion barrier for Na atom make the ReN_2 monolayer a promising anode material. More detailed results will be presented in the following.

Computational methods

The first-principles calculations are done with the projector-augmented wave (PAW) potential method³⁸ as implemented in the Vienna ab initio simulation package software (VASP).³⁹ For all cases, we take the generalized gradient approximation (GGA), accomplished by Perdew, Burke, and Ernzerhof (PBE),⁴⁰ for the exchange-correlation functional. The kinetic energy cutoff of the plane waves is set to 600 eV . For both optimization and static calculation, the Brillouin zone integration is carried out with a $10 \times 10 \times 1$ special Γ -centered k-point mesh following the convention of Monkhorst-Pack.⁴¹ All atomic positions are fully optimized with the conjugate gradient optimization until all the Hellmann-Feynman forces on each atom are less than $0.01 \text{ eV}/\text{\AA}$ and the total energy difference between two successive steps is smaller than 10^{-6} eV . Furthermore, phonon dispersion calculation in terms of the density functional perturbation theory, by using the PHONOPY program,⁴² is performed to ensure the structural stability of the monolayers. We take the $4 \times 4 \times 1$ supercell for calculating the phonon spectra of the 2D structures. In order to make further confirmation, band dispersion calculations with Heyd-Scuseria-Ernzerhof (HSE) hybrid functional^{43–45} are carried out, with the mixing rate of the HF exchange potential being 0.25. The semi-empirical correction scheme of Grimme (DFT-D2)⁴⁶ is employed to evaluate the effect of van der Waals (vdW) interactions on Na/K ion adsorption. In the calculation of Na/K diffusion, we use nudged elastic band (NEB) method to get the ion diffusion barrier.

Results and discussion

Structures and stability

The three-dimensional materials of rhenium dinitride ReN_2 have been synthesized by metathesis reaction under high pressure,⁴⁷ and X-ray Diffraction(XRD) shows that the samples have the same structure as the three-dimensional MoS_2 -like hexagonal structure. A systematical first-principles investigation shows that the three-dimensional MoN_2 -like structure is dynamically stable for ReN_2 and there is a three-dimensional tetragonal structure with lower total energy.^{48,49} In addition, experiment indicates that the three-dimensional ReN_2 may be layered in terms of its compressibility.⁴⁷

As for the two-dimensional structure of ReN_2 monolayer, we consider four possible configurations: T-phase structure, T'-phase structure, H-phase structure, and tetragonal structure. The T-phase structure, which has been found in other two-dimensional materials,⁵⁰ is proved to be unstable for ReN_2 in terms of its phonon spectrum result. Distorted T'-phase structure⁵¹⁻⁵⁴ is also proved to be impossible because our phonon spectrum calculation show that there are very large negative phonon frequencies near the Γ point. Both H-phase structure and tetragonal structure have the phonon spectra without imaginary phonon modes. The total energy of the tetragonal structure is lower than the hexagonal one by 0.33 eV per formula unit. Therefore, the two-dimensional tetragonal structure is stable. It, with space group $\text{P}\bar{4}\text{m}2$, is made up with three atom planes as shown in FIG. 1. The comparative study of spin-polarized and spin-unpolarized calculations show that the tetragonal structure is non-magnetic. Its in-plane lattice parameters a is 3.178 Å, and the vertical distance between the top and bottom nitrogen planes is 1.96 Å. The Re-N bond length $l_{\text{Re-N}}$ is 1.87 Å. The cohesive energy per formula unit is defined as $E_{\text{coh}} = E_{\text{Re}} + E_{\text{N}_2} - E_{\text{ReN}_2}$, where E_{Re} and E_{N_2} are the total energies of isolated Re atom and N_2 molecule. The cohesive energies 6.44 eV is much larger than 1.87 eV for the case of MoN_2 ,⁵⁵ which reveals that the synthesis of the buckled ReN_2 monolayer is accomplishable.

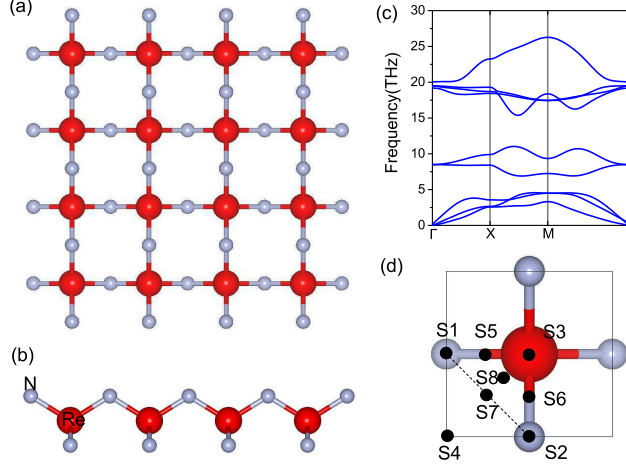


Figure 1: The top (a) and side (b) views of the 2D tetragonal structure, the phonon spectra (c), and the possible sites for Na/K absorption (d) of the ReN_2 monolayer.

In order to analyze the dynamical stability of the 2D tetragonal structure, the phonon spectrum calculations are performed by using the PHONOPY program,⁴² and the calculated results are presented in FIG. 1. It is clear that there are nine phonon branches including three acoustic branches and six optical phonon bands. Non-existence of negative phonon frequencies in FIG. 1 proves the dynamical stability of the 2D tetragonal structures. It can be seen in FIG. 1 that in the vicinity of the Γ point, the acoustical branches show linear dispersion, and the out-of-plane acoustical branch appears to be softer than the other two due to the special mode in the two-dimensional materials.⁵⁶

To inspect the mechanical stability, we calculate the elastic constants of the ReN_2 monolayer: $C_{11} = 107.4 \text{ N/m}$, $C_{22} = 108.0 \text{ N/m}$, $C_{12} = 74.3 \text{ N/m}$, and $C_{66} = 218.8 \text{ N/m}$. The Young's modulus Y is equivalent to 56.3 N/m . For two-dimensional materials, only C_{11} , C_{12} , C_{16} , C_{26} , C_{66} and C_{22} are meaningful quantities, and the criteria of mechanical stability require that $C_{11}C_{22} > C_{12}C_{21}$ and $C_{66} > 0$ ⁵⁷ are satisfied. Thus the tetragonal ReN_2 monolayer has the mechanical stability. Assuming that we have the square flake with the edge length l , the ratio between the out-of plane deformation h induced by its own gravity and the edge length l is $h/l \approx (\rho g l / Y)^{1/3}$, where g being the gravitational acceleration and ρ the density of the two-dimensional material. Here, the density of the ReN_2 monolayer is

$3.54 \times 10^{-6} \text{ kg} \cdot \text{m}^{-2}$, and then we can obtain $h/l \approx (0.62l \times 10^{-12})^{1/3}$ for the ReN_2 monolayer, where l is in micrometer. Even for $10^4 \mu\text{m}^2$ flakes, the ratio is only 3.96×10^{-4} , which is smaller than the previous result of Ca_2N freestanding monolayer (6.31×10^{-4}).⁵⁸ Therefore, the 2D ReN_2 monolayer can keep its stability without the support of a substrate.

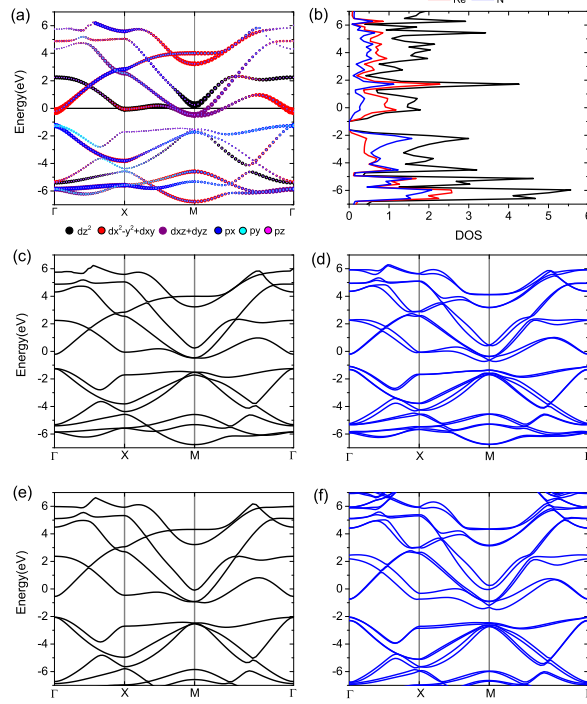


Figure 2: The energy bands (a) and density of states (b) of the ReN_2 monolayer, the PBE energy bands without SOC (c) and with SOC (d), and the HSE energy bands without SOC (e) and with SOC (f).

Electronic structures

The 2D tetragonal structure obeys the S_4 symmetry group. For the electronic wave function of the d orbits, the parity of mirror inversion is even for d_{z^2} , d_{xy} , and $d_{x^2-y^2}$, and odd for d_{xz} and d_{yz} . The band dispersions of the 2D materials without the spin-orbit coupling, with the weights of atomic orbitals indicated, are presented in FIG. 2. The size of symbol is proportional to the weight of the orbital. In the energy spectra, all the N p bands are filled, and the nearly empty bands come from Re d states. Near the Γ point, the band near the

Fermi level is mainly from Re $d_{x^2-y^2}$, and near the X point, the band near the Fermi level consists mainly of Re d_{z^2} and $d_{x^2-y^2}$.

The band structure shows that the two-dimensional ReN_2 monolayer is metallic, but we need to confirm that the system keep metallic feature with HSE calculation or spin-orbit coupling (SOC), because PBE calculation always underestimates the semiconductor gaps and the spin-orbit coupling can open a gap in the transition-metal system. For this purpose, we calculate the energy spectra with HSE with SOC, and the calculated results are presented in FIG. 2. As FIG. 2 shows, the tetragonal ReN_2 monolayer is still metallic. This is advantageous for its applications in Na-ion and K-ion battery technology.

Ion adsorption

A 2×2 supercell of the ReN_2 monolayer is used as the substrate for the adsorption of the Na atom and K atom. After adsorbing a metal atom, the chemical formula of the system can be written as ARe_4N_8 , where A represents Na atom or K atom. The adsorption energy E_a is defined by $E_a = E_{\text{ARe}_4\text{N}_8} - E_{\text{A}} - E_{\text{Re}_4\text{N}_8}$ where E_{A} is the total energy of bulk A metal per atom, and $E_{\text{ARe}_4\text{N}_8}$ and $E_{\text{Re}_4\text{N}_8}$ are the total energy of the Re_4N_8 monolayer with and without A adsorption. According to the symmetry of the Re_4N_8 monolayer, eight possible sites are considered, as shown in FIG. 1(d). Four of the eight sites remain after our geometrical optimization, and their adsorption energies are summarized in TABLE. 1. We can see that the adsorption energies of all the four sites are negative, which means that Na/K atom prefers to be adsorbed on the host material instead of forming a cluster.

The unit cell of the ReN_2 monolayer includes one Re atom, one high-position N atom, and one low-position N atom. According to the adsorption energy, Na/K atom prefers to stay at the position above the low-position N atom (S2 site), and the distance between Na atom and the nitrogen atom right below it is 3.49 Å (3.89 Å for K atom). The adsorption energy at the hollow site (S4) is slightly larger than the adsorption energy at the S2, and much smaller than the adsorption energies at the S1 and S3 sites. Because of the Coulomb

repulsion between Na/K atom and Re atom, the absorbed Na/K atom will not stay at the S3 site. Near the S1 and S4 sites are the high-position N atoms, but near the S2 site are two Re atoms. Thus the Na/K atom prefers to stay at the S2 site (the valley bottom), which can explain the absorption behavior of Na/K atom.

To further understand the absorption of Na/K atom, we make the Bader charge analysis and the results are summarized in TABLE. 1. The existence of charge transference by Na/K atom reveals that the adsorption is chemical, which can be regarded as redox reaction during the battery operation. The calculated charge density difference is showed in FIG. 3, which is defined by $\Delta\rho = \rho(\text{ARe}_4\text{N}_8) - \rho(\text{A}) - \rho(\text{Re}_4\text{N}_8)$. This confirms the existence of chemical adsorption. The larger atom (K atom) reduces the adsorption energy difference between different sites. We also calculate the density of states (DOS) of the Re_4N_8 after absorbing Na/K atom. The calculated results show that the system still keep metallic character, which is advantageous for making electrode materials from the ReN_2 monolayer.

Table 1: The adsorption energy of Na atom ($E_{a\text{Na}}$) and K atom ($E_{a\text{K}}$), and the charge transferred by Na atom (q_{Na}) and K atom (q_{K}).

Sites	$E_{a\text{Na}}$ (eV)	q_{Na} (e)	$E_{a\text{K}}$ (eV)	q_{K} (e)
S1	-0.97	0.88	-1.46	0.88
S2	-1.80	0.87	-2.12	0.88
S3	-1.31	0.88	-1.70	0.88
S4	-1.78	0.84	-1.99	0.88

Key storage parameters

Open circuit voltage (OCV) and theoretical storage capacity are the important parameters to describe the performance of electrode materials. The charge/discharge process of ReN_2 monolayer can be described by $\text{ReN}_2 + x\text{A}^+ + xe^- \leftrightarrow \text{A}_x\text{ReN}_2$. For this reaction, the average open circuit voltage can be defined by $V_{ave} = (E_{\text{ReN}_2} + xE_{\text{A}} - E_{\text{A}_x\text{ReN}_2})/xe$ when we ignore the volume and entropy effects during the alkali metal adsorption process. E_{ReN_2} and $E_{\text{A}_x\text{ReN}_2}$ are the total energies of the ReN_2 monolayer before and after the adsorption of A

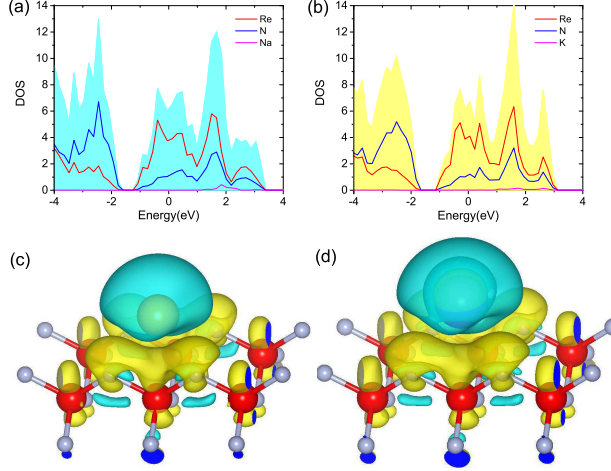


Figure 3: The density of states (DOS) of NaRe_4N_8 (a) and KRe_4N_8 (b). The charge density difference $\Delta\rho$ with the absorption of Na atom (c) and K atom (d) with the isosurface level of $0.001 \text{ e}/\text{\AA}^3$. The yellow area represents the positive charge density difference and the blue area represents the negative one.

(Na or K) atom. In order to calculate the storage capacity, we choose 35\AA as the thickness of vacuum slab to avoid the interaction between neighboring layers. In the process of Na/K intercalation, we calculate the average adsorption energy layer by layer, which is defined by $E_n = (E_{\text{A}_{8n}\text{Re}_4\text{N}_8} - E_{\text{A}_{8(n-1)}\text{Re}_4\text{N}_8} - 8E_{\text{A}})/8$. Here A represents Na or K atom and $E_{\text{A}_{8n}\text{Re}_4\text{N}_8}$ is the total energy of ReN_2 with the adsorption of n A atom layers. Negative E_n means the adsorption of n layers is accessible and we can obtain the maximum storage capacity by $C_M = xF/M_{\text{ReN}_2}$. Here, F is Faraday constant with a value of $26.8 \text{ A h mol}^{-1}$, M_{ReN_2} is the molar mass of ReN_2 per formula unit, and x means the number of A atoms absorbed on the ReN_2 per formula unit.

As shown in FIG. 4, the ReN_2 monolayer can adsorb three layers of Na atoms on each sides for Na-ion batteries, and the maximal storage capacity of the ReN_2 monolayer can reach 751 mA h g^{-1} . The ReN_2 monolayer adsorb only one layer of K atom on each sides and thus its storage capacity is 250 mA h g^{-1} for K-ion batteries. The first Na atom layer is located at the S2 site (above the low-position nitrogen atom), and the average adsorption energy is -1.02 eV , which becomes -0.83 eV for first K atom layer adsorption. Compared to the adsorption energy of one Na/K atom ($-1.80/-2.12 \text{ eV}$), this fact shows that the adsorption

energy of K atom increases faster than that of Na atom while the concentration of Na/K atoms is increasing. Then for the second layer, Na atoms prefer to stay at the S1 site and the average adsorption energy is -0.20 eV, while the positive average adsorption energy for K atom (0.40 eV) reveals that the second K atom layer fails to be absorbed on the ReN_2 monolayer. As for the third layer, Na atoms prefer to be adsorbed at the S4 site and the average adsorption energy becomes -0.08 eV. Three Na atom layers on each sides, in spite of the large mass of the ReN_2 , make the ReN_2 monolayer a high-capacity anode material. The average open-circuit voltage decreases from 1.0 to 0.4 V with the increase of the adsorbed Na concentration from 8 to 24 atoms on the 2×2 supercell. The open circuit voltage for K-ion batteries is 0.83 V with 8 atoms on the 2×2 supercell. In the process of intercalation of Na (K) atom, the change of lattice parameter is only 3.2% (3.8%), which is propitious to achieve the rechargeable batteries.

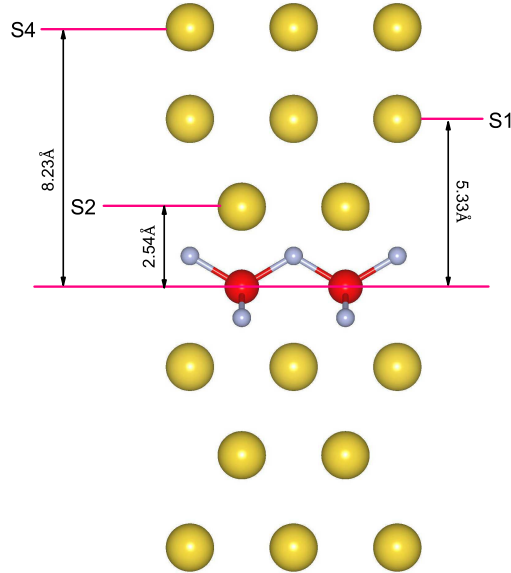


Figure 4: The side view of the atomic structure of Na-intercalated ReN_2 monolayer, where up to three Na layers can be absorbed.

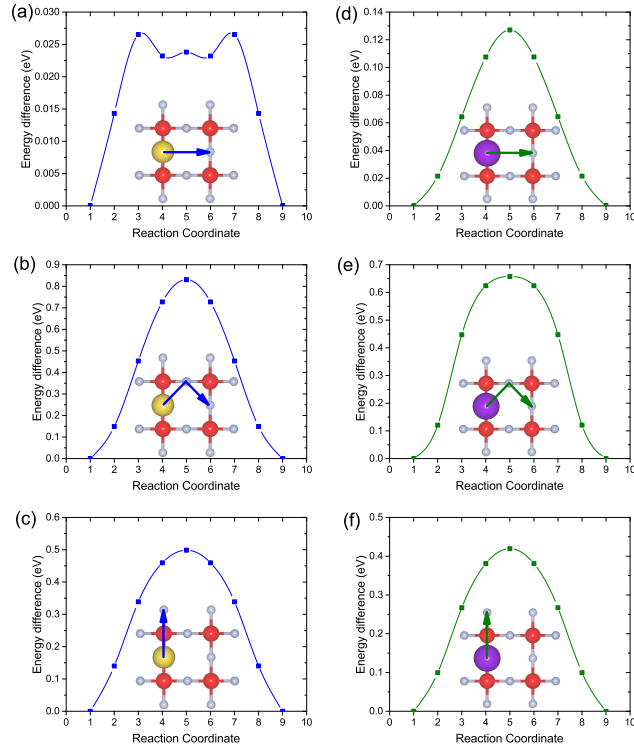


Figure 5: Energy profiles of Na diffusion on path 1 (a), path 2 (b), and path 3 (c), and those of K diffusion on path 1 (d), path 2 (e), and path 3 (f). The inserted figures show the corresponding diffusion pathways.

Ion diffusion

The fast charging and discharging processes need the fast ion diffusion. The ion diffusion depends on the temperature-dependent molecular transition rate D , which is proportional to $\exp(-E_d/k_B T)$, where E_d , k_B , and T are the diffusion barrier, Boltzmann's constant, and temperature, respectively. A low diffusion barrier means a fast charging/discharging process for ion batteries. Three possible diffusion paths are taken into consideration, and the calculated results are shown in FIG. 5. The diffusion barrier of the path 1 is 0.027 eV and 0.127 eV for Na-ion and K-ion batteries, respectively, which is the lowest of three possible circumstances. It can be explained by the existence of hollow space in the monolayer which reduces the influence of the energy variation at the different sites. The extremely low diffusion barrier of Na atom can bring to ultrafast charging/discharging cycles in the Na-ion batteries.

It is noted that Na/K diffusion on the ReN_2 monolayer is quite anisotropic. Coming from the S1 site, Na atom will encounter the hollow space along path1 or relatively high-position Re atom along path 3. It brings to the great anisotropy between the diffusion barriers along the two orthogonal directions, and the ratio is $E_{d3}/E_{d1} \approx 18$ for Na atom or $E_{d3}/E_{d1} \approx 3$ for K atom. The anisotropy is greater than phosphorene (the ratio is 8)⁵⁹ and can achieve the unusual transports along the different directions in the these systems.

Comparison with others

It is interesting to compare the ReN_2 with other two-dimensional materials for ion batteries. For Na-ion batteries, the data are summarized in TABLE. 2. It can be seen that the maximal storage capacity of the ReN_2 monolayer is smaller than those of borophene,⁶⁰ Ca_2N ,³⁷ phosphorene,⁵⁹ and MoN_2 monolayer,⁶¹ but better than those most of transition-metal dichalcogenides, MXenes, and so on. For K-ion batteries, the maximum capacity of the ReN_2 monolayer (250 mA h g⁻¹) is comparable to those of GeS (256 mA h g⁻¹),⁶³ Mo_2C (smaller than 263 mA h g⁻¹),³⁴ and Ti_3C_2 (191.8 mA h g⁻¹),³⁵ but smaller than those of

MoN₂ (432 mA h g⁻¹)⁶¹ and BP (570 mA h g⁻¹).⁶² The ReN₂ monolayer is better serving as Na-ion storage materials than as K-ion ones. Compared to other two-dimensional materials, the ReN₂ have the extremely low Na ion diffusion barrier that is lower than those of other 2D materials except Sr₂N monolayer³⁷ and Mo₂C monolayer.³⁴ Actually, the maximum capacity of the ReN₂ monolayer is twice or five times that of Sr₂N or Mo₂C. The K-ion diffusion barrier of the ReN₂ monolayer (0.127 eV) is smaller than those of MoN₂ (0.49 eV)⁶¹ and BP (0.155 eV),⁶² and larger than those of Mo₂C (0.015 eV),³⁴ GeS (0.050 eV),⁶³ and Ti₃C₂ (0.103 eV).³⁵ Very importantly, the ReN₂ monolayer have both very high storage capacity and extremely low ion diffusion barrier, which makes it promising electrode materials for Na-ion batteries.

Table 2: The maximum capacity C_M and diffusion barrier E_d of two-dimensional electrode materials for Na-ion batteries.

	C_M (mA h g ⁻¹)	E_d (eV)	Ref.
ReN ₂	751	0.027	This work
β_{12} borophene	1984	0.33	Ref. ⁶⁰
χ_3 borophene	1240	0.34	Ref. ⁶⁰
Ca ₂ N	1138	0.08	Ref. ³⁷
Phosphorene	865	0.04	Ref. ⁵⁹
MoN ₂	864	0.56	Ref. ⁶¹
GeS	512	0.09	Ref. ⁶³
TiS ₂	339	0.22	Ref. ⁶⁴
Sr ₂ N	283	0.016	Ref. ³⁷
NbS ₂	263	0.07	Ref. ⁶⁴
BP	143	0.217	Ref. ⁶²
Mo ₂ C	132	0.019	Ref. ³⁴

Conclusion

In summary, we have studied the ReN₂ monolayer as new 2D materials and explored its application in Na-ion and K-ion batteries by first-principles calculation. The calculated results show that the two-dimensional ReN₂ monolayer is promising as electrode materials: (1) it keeps metallic feature before and after the adsorption of Na/K atom and thus has the

good electric conductivity; (2) the small lattice changes during the intercalation reveals the good recyclability; (3) the maximum storage capacity of the ReN_2 monolayer reaches 751 mA h g^{-1} for Na-ion batteries, which is quite high among two-dimensional electrode materials to date; (4) the low diffusion barriers (0.027 eV for Na and 0.127 eV for K) can make the charging/discharging cycles fast. Therefore, our works show that the ReN_2 monolayer is promising as electrode materials for Na/K-ion batteries.

Acknowledgement

This work is supported by the Nature Science Foundation of China (No. 11574366), by the Strategic Priority Research Program of the Chinese Academy of Sciences (Grant No.XDB07000000), and by the Department of Science and Technology of China (Grant No. 2016YFA0300701).

References

- (1) Novoselov, K. S.; Geim, A. K.; Morozov, S. V.; Jiang, D.; Zhang, Y.; Dubonos, S. V.; Grigorieva, I. V.; Firsov, A. A. Electric Field Effect in Atomically Thin Carbon Films. *Science* **2004**, 306, 666-669.
- (2) Novoselov, K. S.; Geim, A. K.; Morozov, S. V.; Jiang, D.; Katsnelson, M. I.; Grigorieva, I. V.; Dubonos, S. V.; Firsov, A. A. Two-dimensional gas of massless Dirac fermions in graphene. *Nature* **2005**, 438, 197-200.
- (3) Geim A. K.; Novoselov, K. S. The rise of graphene. *Nat. Mater.* **2007**, 6, 183-191.
- (4) Castro Neto, A. H.; Guinea, F.; Peres, N. M. R.; Novoselov, K. S.; Geim, A. K. The electronic properties of graphene. *Rev. Mod. Phys.* **2009**, 81, 109-162.
- (5) Radisavljevic, B.; Radenovic, A.; Brivio, J.; Giacometti, V.; Kis, A. Single-layer MoS_2 transistors. *Nat. Nanotech.* **2011**, 6, 147-150.

- (6) Li, L.; Yu, Y.; Ye, G. J.; Ge, Q.; Ou, X.; Wu, H.; Feng, D.; Chen, X. H.; Zhang, Y. Black phosphorus field-effect transistors. *Nat. Nanotech.* **2014**, 9, 372-377.
- (7) Yin, Z.; Li, H.; Li, H.; Jiang, L.; Shi, Y.; Sun, Y.; Lu, G.; Zhang, Q.; Chen, X.; Zhang, H. Single-Layer MoS₂ Phototransistors. *ACS Nano* **2012**, 6, 74-80.
- (8) Xu, K.; Wang, Z.; Wang, F.; Huang, Y.; Wang, F.; Yin, L.; Jiang, C.; He, J. Ultrasensitive Phototransistors Based on Few-Layered HfS₂. *Adv. Mater.* **2015**, 27, 7881-7887.
- (9) Li, M. Y.; Shi, Y.; Cheng, C. C.; Lu, L. S.; Lin, Y. C.; Tang, H. L.; Tsai, M. L.; Chu, C. W.; Wei, K. H.; He, J. H. Epitaxial growth of a monolayer WSe₂-MoS₂ lateral p-n junction with an atomically sharp interface. *Science* **2015**, 349, 524-528.
- (10) Peng, B.; Yu, G.; Liu, X.; Liu, B.; Liang, X.; Bi, L.; Deng, L.; Sum, T. C.; Loh, K. P. Ultrafast charge transfer in MoS₂/WSe₂ p/n Heterojunction. *2D Mater.* **2016**, 3, 025020.
- (11) Acerce, M.; Voiry, D.; Chhowalla, M. Metallic 1T phase MoS₂ nanosheets as supercapacitor electrode materials. *Nat. Nanotech.* **2015**, 10, 313-318.
- (12) Yang, H.; Wang, N.; Xu, Q.; Chen, Z.; Ren, Y.; Razal, J. M.; Chen, J. Fabrication of graphene foam supported carbon nanotube/polyaniline hybrids for high-performance supercapacitor applications. *2D Mater.* **2014**, 1, 034002.
- (13) Dunn, B.; Kamath, H.; Tarascon, J. M. Electrical Energy Storage for the Grid: A Battery of Choices. *Science* **2011**, 334, 928-935.
- (14) Quesnel, E.; Roux, F.; Emieux, F.; Faucherand, P.; Kymakis, E.; Volonakis, G.; Giustino, F.; Martin-Garcia, B.; Moreels, I.; Gursel, S. A. Graphene-based technologies for energy applications, challenges and perspectives. *2D Mater.* **2015**, 2, 030204.
- (15) Tarascon J.; Armand, M. Issues and challenges facing rechargeable lithium batteries. *Nature* **2001**, 414, 359-367.

- (16) Idota, Y.; Kubota, T.; Matsufuji, A.; Maekawa Y.; Miyasaka, T. Tin-Based Amorphous Oxide: A High-Capacity Lithium-Ion-Storage Material. *Science* **1997**, 276, 1395-1397.
- (17) Nam, K. T.; Kim, D. W.; Yoo, P. J.; Chiang, C. Y.; Meethong, N.; Hammond, P. T.; Chiang, Y. M.; Belcher, A. M. Virus-enabled synthesis and assembly of nanowires for lithium ion battery electrodes. *Science* **2006**, 312, 885-888.
- (18) Zou, F.; Hu, X.; Qie, L.; Jiang, Y.; Xiong, X.; Qiao Y.; Huang, Y. Facile synthesis of sandwiched Zn_2GeO_4 -graphene oxide nanocomposite as a stable and high-capacity anode for lithium-ion batteries. *Nanoscale* **2014**, 6, 924-930.
- (19) Liu, M.; He, Y.; Lv, W.; Zhang, C.; Du, H.; Li, B.; Yang Q.; Kang, F. High catalytic activity of anatase titanium dioxide for decomposition of electrolyte solution in lithium ion battery. *J. Power Sources* **2014**, 268, 882-886.
- (20) Sun, X.; Yan, C.; Chen, Y.; Si, W.; Deng, J.; Oswald, S.; Liu L.; Schmidt, O. G. Three-dimensionally "curved" NiO nanomembranes as ultrahigh rate capability anodes for Li-ion batteries with long cycle lifetimes. *Adv. Energy Mater.* **2014**, 4, 1300912.
- (21) Wang, J.; Zhang, Q.; Li, X.; Zhang, B.; Mai L.; Zhang, K. Smart construction of three-dimensional hierarchical tubular transition metal oxide core/shell heterostructures with high-capacity and long-cycle-life lithium storage. *Nano Energy* **2015**, 12, 437-446.
- (22) Qian, X.; Gu, X.; Dresselhaus, M. S.; Yang, R. Anisotropic Tuning of Graphite Thermal Conductivity by Lithium Intercalation. *J. Phys. Chem. Lett.* **2016**, 7, 4744-4750.
- (23) Shi, L.; Zhao, T.; Xu, A.; Xu, J. Ab initio prediction of a silicene and graphene heterostructure as an anode material for Li- and Na-ion batteries. *J. Mater. Chem. A* **2016**, 4, 16377-16382.
- (24) Etacheri, V.; Marom, R.; Elazari, R.; Salitra, G.; Aurbach, D. Challenges in the development of advanced Li-ion batteries: A review. *Energy Environ. Sci.* **4**, 3243 (2011).

- (25) Reddy, M.; Subba Rao G.; Chowdari, B. Metal oxides and oxysalts as anode materials for Li ion batteries. *Chem. Rev.* **2013**, 113, 5364-5457.
- (26) McDowell, M. T.; Lee, S. W.; Nix, W. D.; Cui, Y. 25th anniversary article: Understanding the lithiation of silicon and other alloying anodes for lithium-ion batteries. *Adv. Mater.* **2013**, 25, 4966-4985.
- (27) Larcher, D.; Tarascon, J. Towards greener and more sustainable batteries for electrical energy storage. *Nat. Chem.* **2015**, 7, 19-29.
- (28) Yamamoto, T.; Nohira, T.; Hagiwara, R.; Fukunaga, A.; Sakai, S.; Nitta, K.; Inazawa, S. Charge-discharge behavior of tin negative electrode for a sodium secondary battery using intermediate temperature ionic liquid sodium bis(fluorosulfonyl) amide-potassium bis(fluorosulfonyl)amide. *J. Power Sources* **2012**, 217, 479-484.
- (29) Pollak, E.; Geng, B.; Jeon, K.-J.; Lucas, I. T.; Richardson, T. J.; Wang, F.; Kostecki, R. The interaction of Li⁺ with single-layer and few-layer graphene. *Nano Lett.* **2010**, 10, 3386-3388.
- (30) Tang, Q.; Zhou, Z.; Chen, Z. Graphene-related nanomaterials: Tuning properties by functionalization. *Nanoscale* **2013**, 5, 4541-4583.
- (31) David, L.; Bhandavat R.; Singh, G. MoS₂/graphene composite paper for sodium-ion battery electrodes. *ACS Nano* **2014**, 8, 1759-1770.
- (32) Bhandavat, R.; David, L.; Singh, G. Synthesis of surface-functionalized WS₂ nanosheets and performance as li-ion battery anodes. *J. Phys. Chem. Lett.* **2012**, 3, 1523-1530.
- (33) Jing, Y.; Zhou, Z.; Cabrera, C.; Chen, Z. Metallic VS₂ monolayer: A promising 2D anode material for lithium ion batteries. *J. Phys. Chem. C* **2013**, 117, 25409-25413.

- (34) Sun, Q.; Dai, Y.; Ma, Y.; Jing, T.; Wei, W.; Huang, B. Ab Initio Prediction and Characterization of Mo₂C Monolayer as Anodes for Lithium-Ion and Sodium-Ion Batteries. *J. Phys. Chem. Lett.* **2016**, 7, 937-943.
- (35) Er, D.; Li, J.; Naguib, M.; Gogotsi, Y.; Shenoy, V. Ti₃C₂ MXene as a high capacity electrode material for metal (Li, Na, K, Ca) ion batteries. *ACS Appl. Mater. Interfaces* **2014**, 6, 11173-11179.
- (36) Hu, J.; Xu, B.; Ouyang, C.; Yang, S. A.; Yao, Y. Investigations on V₂C and V₂CX₂ (X = F, OH) monolayer as a promising anode material for Li ion batteries from first-principles calculations. *J. Phys. Chem. C* **2014**, 118, 24274-24281.
- (37) Hu, J.; Xu, B.; Yang, S. A.; Guan, S.; Ouyang, C.; Yao, Y. 2D Electrides as Promising Anode Materials for Na-Ion Batteries from First-Principles Study. *ACS Appl. Mater. Interfaces* **2015**, 7, 24016-24022.
- (38) Blochl, P. E. Projector augmented-wave method. *Phys. Rev. B* **1994**, 50, 17953-17979.
- (39) Kresse G.; Furthmüller, J. Efficient iterative schemes for ab initio total-energy calculations using a plane-wave basis set. *Phys. Rev. B* **1996**, 54, 11169-11186.
- (40) Perdew, J. P.; Burke, K.; Ernzerhof, M. Generalized Gradient Approximation Made Simple. *Phys. Rev. Lett.* **1996**, 77, 3865-3868.
- (41) Monkhorst, H. J.; Pack, J. D. Special points for Brillouin-zone integrations. *Phys. Rev. B* **1976**, 13, 5188-5192.
- (42) Togo, A.; Oba, F.; Tanaka, I. First-principles calculations of the ferroelastic transition between rutile-type and CaCl₂-type SiO₂ at high pressures. *Phys. Rev. B* **2008**, 78, 134106.
- (43) Heyd, J.; Scuseria, G. E.; Ernzerhof, M. Hybrid functionals based on a screened Coulomb potential. *J. Chem. Phys.* **2003**, 118, 8207-8215.

- (44) Krukau, A. V.; Vydrov, O. A.; Izmaylov, A. F.; Scuseria, G. E. Influence of the exchange screening parameter on the performance of screened hybrid functionals. *J. Chem. Phys.* **2006**, 125, 224106.
- (45) Mori-Sanchez, P.; Cohen, A. J.; Yang, W. Localization and Delocalization Errors in Density Functional Theory and Implications for Band-Gap Prediction. *Phys. Rev. Lett.* **2008**, 100, 146401.
- (46) Grimme, S. Semiempirical GGA-type density functional constructed with a long-range dispersion correction. *J. Comput. Chem.* **2006**, 27, 1787.
- (47) Kawamura, F.; Yusa, H.; Taniguchi, T. Synthesis of rhenium nitride crystals with MoS₂ structure. *Appl. Phys. Lett.* **2012**, 100, 251910.
- (48) Wang, Y.; Yao, T.; Yao, J. L.; Zhang, J.; Gou, H. Does the real ReN₂ have the MoS₂ structure? *Phys. Chem. Chem. Phys.* **2013**, 15, 183-187.
- (49) Yan, H.; Zhang, M.; Wei, Q.; Guo, P. Theoretical study on tetragonal transition metal dinitrides from first principles calculations. *J. Alloys Compounds* **2013**, 581, 508-514.
- (50) Chhowalla, M.; Shin, H. S.; Eda, G.; Li, L. J.; Loh, K. P.; Zhang, H. The chemistry of two-dimensional layered transition metal dichalcogenide nanosheets. *Nat. Chem.* **2013**, 5, 263-275.
- (51) Calandra, M. Chemically exfoliated single-layer MoS₂: Stability, lattice dynamics, and catalytic adsorption from first principles. *Phys. Rev. B* **88**, 245428 (2013).
- (52) Tongay, S.; Sahin, H.; Ko, C.; Luce, A.; Fan, W.; Liu, K.; Zhou, J.; Huang, Y. S.; Ho, C. H.; Yan, J.; Ogletree, D. F.; Aloni, S.; Ji, J.; Li, S.; Li, J.; Peeters, F. M.; Wu, J. Monolayer behaviour in bulk ReS₂ due to electronic and vibrational decoupling. *Nat. Commun.* **2014**, 5, 3252.

- (53) D. H. Keum, S. Cho, J. H. Kim, D. H. Choe, H. J. Sung, M. Kan, H. Kang, J. Y. Hwang, S. W. Kim, H. Yang, K. J. Chang, and Y. H. Lee, Nat. Phys. **11**, 482 (2015).
- (54) Ersan, F.; Cahangirov, S.; Gokoglu, G.; Rubio, A.; Akturk, E. Stable monolayer honeycomb-like structures of RuX_2 ($X = \text{S}, \text{Se}$). Phys. Rev. B **2016**, 94, 155415.
- (55) Wu, H.; Qiana, Y.; Luo, R.; Tan, W. A theoretical study on the electronic property of a new two-dimensional material molybdenum dinitride. Phys. Lett. A **2016**, 380, 768-772.
- (56) Liu, F.; Ming, P.; Li, J. Ab initio calculation of ideal strength and phonon instability of graphene under tension. Phys. Rev. B **2007**, 76, 064120.,
- (57) R. C. Andrew, R. E. Mapasha, A. M. Ukpang, and N. Chetty, Mechanical properties of graphene and boronitrene. Phys. Rev. B **2012**, 85, 125428.
- (58) Zhao, S.; Li, Z.; Yang, J. Obtaining Two-Dimensional Electron Gas in Free Space without Resorting to Electron Doping: An Electride Based Design. J. Am. Chem. Soc. **2014**, 136, 13313-13318.
- (59) Kulish, V. V.; Malyi, O. I.; Persson, C.; Wu, P. Phosphorene as an anode material for Na-ion batteries: a first-principles study. Phys. Chem. Chem. Phys. **2015**, 17, 13921-13928.
- (60) Zhang, X.; Hu, J.; Cheng, Y.; Yang, H. Y.; Yao, Y.; Yang, S. A. Borophene as an extremely high capacity electrode material for Li-ion and Na-ion batteries. Nanoscale **2016**, 8, 15340-15347.
- (61) Zhang, X.; Yu, Z.; Wang, S. S.; Guan, S.; Yang, H. Y.; Yao, Y.; Yang, S. A. Theoretical prediction of MoN_2 monolayer as a high capacity electrode material for metal ion batteries. J. Mater. Chem. A **2016**, 4, 15224-15231.

- (62) Jiang, H. R.; Shyy, W.; Liu, M.; Wei, L.; Wu, M. C.; Zhao, T. S. Boron phosphide monolayer as a potential anode material for alkali metal-based batteries. *J. Mater. Chem. A* **2017**, 5, 672-679.
- (63) Li, F.; Qu Y.; Zhao, M. Germanium sulfide nanosheet: a universal anode material for alkali metal ion batteries. *J. Mater. Chem. A* **2016**, 4, 8905-8912.
- (64) Yang, E.; Ji, H.; Jung, Y. Two-Dimensional Transition Metal Dichalcogenide Mono layers as Promising Sodium Ion Battery Anodes. *J. Phys. Chem. C* **2015**, 119, 26374-26380.